Eur. J. Mineral., 37, 91–99, 2025
https://doi.org/10.5194/ejm-37-91-2025

European Journal of Mineralogy
Open Access

Extrinsic and intrinsic strength of amorphous olivine films

Jens Jarnot[1], Ralf Dohmen[2], Claus O. W. Trost[3], Christian Mitterer[1], Patrick Cordier[4,5], and Oleksandr Glushko[1]

[1]Department of Materials Science, Montanuniversität Leoben, Franz-Josef Straße 18, 8700 Leoben, Austria
[2]Institute of Geology, Mineralogy, and Geophysics, Ruhr University Bochum, Universitätsstr. 150, 44801 Bochum, Germany
[3]Erich Schmid Institute for Materials Science of the Austrian Academy of Sciences, Jahnstr. 12, 8700 Leoben, Austria
[4]Univ. Lille, CNRS, INRAE, Centrale Lille, UMR 8207–UMET–Unité Matériaux et Transformations, 59655 Lille, France
[5]Institut Universitaire de France, 75005 Paris, France

Correspondence: Patrick Cordier (patrick.cordier@univ-lille.fr) and Oleksandr Glushko (oleksandr.glushko@unileoben.ac.at)

Received: 21 September 2024 – Revised: 13 December 2024 – Accepted: 19 December 2024 – Published: 25 February 2025

Abstract. Nanoscale amorphous olivine (a-olivine) intracrystalline layers, which can form in olivine polycrystals under high stress, has the potential to influence the mechanical properties of the rock in the vicinity of the brittle–ductile transition. It is therefore essential to determine the mechanical properties, in particular the strength, of these a-olivine films. To this end, we investigate the tensile deformation and fracture of a-olivine thin films deposited on a polymer substrate. Typical brittle fracture in the form of numerous long, straight cracks that are parallel to each other is observed during a tensile test. Using in situ measurements of electrical resistance, the critical strain required for the generation of the first cracks was measured at 0.8 %. A combination of in situ straining with optical microscopy and subsequent digital image correlation enables direct measurements of local strains within the unfractured film regions. It is demonstrated that a-olivine can withstand tensile strains of at least 2 %, which leads to an estimated intrinsic strength of 1.8 GPa. The results presented should contribute to a more comprehensive understanding of the mechanical behavior of olivine-rich rocks affected by grain boundary amorphization.

1 Introduction

The presence of amorphous material, such as silicate melt, in seismically and aseismically sheared rocks has been well documented and is observed in deformation experiments (Andrault et al., 1995; Goldsby and Tullis, 2002; Hayward et al., 2016; Niemeijer et al., 2011; Pec et al., 2012; Yund et al., 1990). Natural formation of the amorphous phase can also be explained by frictional melting (Austrheim and Andersen, 2004; Obata and Karato, 1995; Scambelluri et al., 2017) or by severe mechanical deformation without significant heating (Janssen et al., 2010; Kaneki et al., 2020; Pec et al., 2012; Wenk, 1978). The present study is inspired by a recent experimental investigation into the deformation of olivine aggregates at relatively low temperatures (around 1000 °C, i.e., ca. $0.6\,T/T_m$) and high stress, which revealed a remarkably early stage of solid-state amorphization (without melting) confined to the grain boundaries (Gasc et al., 2019; Samae et al., 2021). Such a microstructure can have important consequences for the mechanical properties since the presence of an intergranular glassy phase can be the cause of localized brittle behavior at grain boundaries (Gasc et al., 2019) when the temperature is lower than the glass transition temperature (1263 ± 10 °C for amorphous olivine; Richet et al., 1993). On the other hand, it has been shown for metallic

alloys that amorphous layers at the grain boundaries can lead to better ductility and toughness (Pan and Rupert, 2015). In order to understand and predict the behavior of bulk polycrystalline olivine containing amorphous phase, the mechanical properties of amorphous olivine (a-olivine) must be assessed.

Little is known about the mechanical properties of a-olivine since it has never been observed in bulk form. Amorphous olivine at grain boundaries has the thickness of only a few nanometers (Samae et al., 2021), which makes reliable measurements of its mechanical properties problematic. However, a-olivine can be obtained in a thin-film form by means of pulsed laser deposition (PLD) technique employing crystalline olivine as a target. A nanoindentation study of a-olivine thin film (Baral et al., 2021) allowed us to measure Young's modulus and the strain rate sensitivity exponent of a-olivine using indentation relaxation reaching strain rates below $10^{-6}\,s^{-1}$. This field has recently been extended by on-chip tensile experiments (Coulombier et al., 2024), which have shown that the same deformation mechanism operates during the viscoelastic relaxation of a-olivine under strain rates as low as $10^{-12}\,s^{-1}$.

Since natural a-olivine is strongly confined between the crystalline olivine grains (Samae et al., 2021), characterization of its *intrinsic* strength is of particular interest; however, this is a challenging task from an experimental point of view. In the case of crystalline films, tensile testing with in situ synchrotron X-ray diffraction characterization could be a very effective method to capture the evolution of lattice strains and deduce the intrinsic strength of thin films (Jörg et al., 2017). However, amorphous materials do not exhibit narrow and clearly defined diffraction peaks, which makes the usage of diffraction-based methods less effective. A nanomechanical testing approach (Coulombier et al., 2024; Kiener and Misra, 2023), which can be applied to a-olivine films, requires fabrication of freestanding nanoscale specimens whose mechanical behavior is influenced by the sample preparation procedure, geometry, and testing setup. Additionally, bulk and surface defects, which can act as stress concentrators, will inevitably influence the measured strength and observed fracture behavior, particularly since glassy olivine at room temperature is expected to show intrinsically brittle behavior (Coulombier et al., 2024; Darot et al., 1985; Druiventak et al., 2011; Kranjc et al., 2020). It is therefore imperative to exercise caution when considering the applicability of any test results to the actual mechanical behavior of strongly confined a-olivine layers in an olivine aggregate. In other words, experimental designs enabling the measurement of the intrinsic mechanical properties of a-olivine, which are not influenced by the sample geometry, properties of testing setup, defect type, concentration and distribution, etc., are required.

In this study, we adopt an alternative approach to characterizing the intrinsic strength of a-olivine by investigating the behavior of a-olivine thin films deposited by PLD on a polymer substrate. By conducting tensile tests in situ under an optical microscope in conjunction with digital image correlation, we determine the maximum strain a-olivine can withstand without fracturing and thereby estimate the lower bound of its intrinsic strength value.

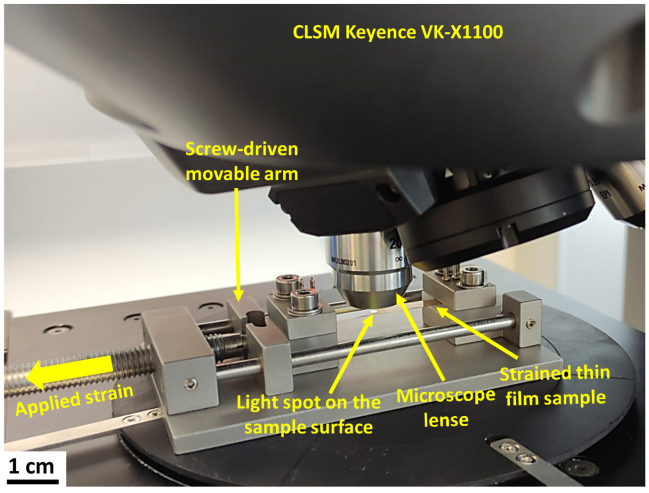

Figure 1. Photograph of the arrangement for the tensile straining experiment under the CLSM.

2 Materials and methods

In order to deposit a-olivine thin films by PLD, polycrystalline pellets of synthetic olivine with a nominal composition of $Mg_{1.8}Fe_{0.2}SiO_4$ were ablated using a pulsed laser beam with a frequency of 10 Hz, a wavelength of 193 nm, a target-to-substrate distance of 50 mm, and a laser fluence of 1–2 $J\,cm^{-2}$. The main principle of PLD and various examples of thin-film depositions were provided by Dohmen et al. (2002) for a former PLD system in Bochum. The new depositions were performed using a PLD system designed and fabricated by SURFACE systems + technology GmbH & Co. KG, Hückelhoven, Germany. The deposition rates were in the range of 3–4 $nm\,min^{-1}$. The depositions were performed at a background vacuum pressure of approximately 1×10^{-4} Pa at room temperature. Under these conditions, the silicate film of an olivine-like composition is amorphous and chemically homogeneous (Baral et al., 2021; Dohmen et al., 2002). The depositions were performed on 50 µm thick polyimide Upilex 50S substrates with dimensions of $5 \times 5\,cm^2$. The PLD setup does not allow the rotation of the substrate during deposition, and the plasma jet coming out of the target is relatively small compared to the substrate. Therefore, each substrate comprises a circular area of approximately 20 mm in diameter and 100 nm in thickness, wherein deposition is most concentrated. In the surrounding area, the thickness gradually decreases until it reaches zero within a range of 10–20 mm from the edges of the central circular area.

For tensile experiments, single stripes with dimensions of 4 mm × 40 mm were cut out from the coated substrates using a knife, with the central circular area positioned in the center of the stripe. In this way, it was ensured that subsequent characterization is applied to film portions with the same thickness. Tensile tests were performed under a confocal laser scanning microscope (CLSM) on as-deposited a-olivine films using a custom-made, manual, screw-driven straining setup, depicted in Fig. 1, and described in more details in the Supplement. The thin-film sample is fixed between a rigid and a movable arm of the device. Strain is applied in discrete steps by manual movement of the movable arm, as shown schematically in Fig. 1. The surface images were recorded using a KEYENCE VK-X1100 CLSM at zero strain and after each applied straining step. The applied global strain was measured directly on the sample surface by recording the change in distance between two characteristic points visible at low magnification at each straining step. The applied strain rate is estimated to be on the order of 10^{-2}–$10^{-3}\,s^{-1}$. A total of six specimens were tested in situ under CLSM, and they demonstrated similar deformation and fracture behavior. An overview of the tested samples and applied straining steps is provided in the Supplement.

The crack density was calculated as the number of cracks per unit length crossing a straight line parallel to the loading direction on the basis of CLSM images.

To enable the characterization of film fracture through in situ resistance measurements, a thin gold coating with an estimated thickness of approximately 10 nm was sputter-deposited on the surface of the a-olivine. Subsequently, tensile tests with in situ resistance measurements in four-point probe geometry were conducted on these specimens using an MTS Tytron 250 tensile testing device which was equipped with probes incorporated in the grips. The principles of tensile testing of polymer-supported specimens with in situ resistance measurements are described in greater detail in Glushko and Cordill (2016). The dimensions of the tensile specimens were $4 \times 40\,mm^2$ with a gauge length of 10 mm. Three samples were tested, demonstrating excellent reproducibility of the resistance behavior.

Digital image correlation (DIC) was conducted with the free version of GOM Correlate 2016 software relying on the natural speckle pattern of the sample surface. To calculate the local surface strain using DIC, the images with the resolution of 1024 × 768 pixels were utilized, corresponding to a pixel size of approximately 90 nm. The subset size and step size of the DIC analysis were 15 and 7 pixels, respectively.

Scanning electron microscopy (SEM) was performed on an FEI Versa 3D focused iron beam (FIB)–SEM workstation using specimens coated with gold. The thickness of the a-olivine film was measured to be approximately 105 nm through the analysis of an SEM image of a film cross-section prepared by FIB.

3 Results and discussion

Figure 2 depicts CLSM optical images of the surface of polymer-supported a-olivine films. The corresponding movie, which includes each loading and unloading step, is provided in the supplementary video available online (see "Video supplement"). No cracks were observed up to the applied strain of 0.8 % (Fig. 2a, d). At the strain of 1.3 % (Fig. 2b, e), multiple straight and parallel cracks appear, and the crack density increases with increasing applied strain (Fig. 2c, f). This behavior is typical of intrinsically brittle materials (Jörg et al., 2017; Latella et al., 2007; Park et al., 2010; Peng et al., 2011).

At higher strains (> 10 %), local delaminations, also referred to as buckles, begin to emerge due to the compressive stresses induced by Poisson contraction. A post-mortem SEM image illustrating the presence of cracks and a buckle in the specimen, which was strained to 11.7 %, is presented in Fig. 3. The SEM analysis does not provide any evidence of plastic deformation, such as shear bands or necking, which suggests that the fracture was brittle. As can be seen in the magnified image of the buckle (Fig. 3b), cracks are present within the curved surface of the buckle, confirming that a-olivine is unable to accommodate bending strains without fracture at room temperature and pressure. On the opposite side of the same strip, a flake is observed that is attributed to a fractured and popped-out buckle due to its characteristic triangular shape (Fig. 3a). All other buckles observed in SEM were either cracked, partially fractured, or completely fractured. It can, therefore, be concluded that at room temperature and an applied straining rate in the range of 10^{-2}–$10^{-3}\,s^{-1}$, a-olivine behaves as a brittle material, exhibiting fracture immediately following the elastic deformation regime.

To ascertain the critical strain at which the film begins to crack – the crack onset strain (COS) – a series of tensile tests with in situ resistance measurements were conducted. As a-olivine is not electrically conductive, a gold layer with a thickness of approximately 10 nm was deposited by sputter coating on the a-olivine film prior to testing. The cracking of the olivine film immediately induces rapid growth of the electrical resistance measured in situ, as demonstrated in Fig. 4 (blue curve). A COS value of approximately 0.8 % was determined from the in situ resistance curve. The evolution of linear crack density with increasing strain, as determined from the CLSM images, is also illustrated in Fig. 4 (black symbols and curve). As can be observed, following the attainment of the critical strain, the crack density increases with increasing strain, reaching a plateau at approximately 8 % strain. The saturation of the crack density in polymer-supported films with increasing strain is a well-documented phenomenon that can be explained by the shear lag model (Ahmed et al., 2011; Hsueh and Yanaka, 2003). Formation of a crack results in stress relaxation in the region immediately adjacent to its edges. Therefore, the subsequent crack may

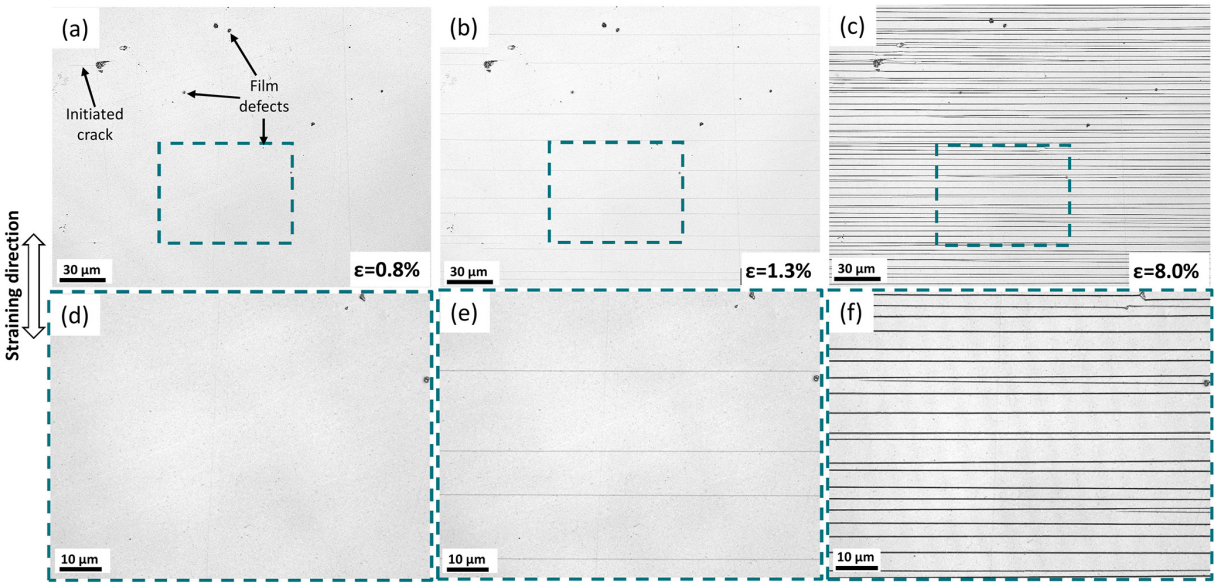

Figure 2. CLSM images of the surface of the polymer-supported a-olivine film with a thickness of about 100 nm during in situ straining for the applied strains of 0.8 % **(a)**, 1.3 % **(b)**, and 8.0 % **(c)**. The enlarged images from the dashed rectangles in **(a)**–**(c)** are depicted in **(d)**–**(f)**, respectively. The first initiated crack and examples of film defects are depicted in **(a)**.

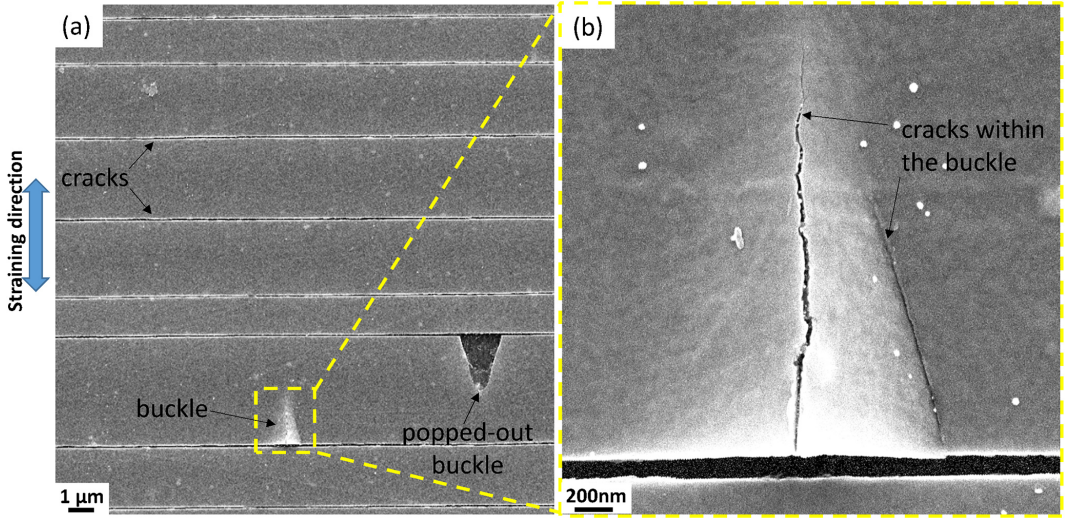

Figure 3. Post-mortem SEM image of a polymer-supported a-olivine film after straining to 11.6 % **(a)** and the corresponding enlarged image of a buckle **(b)**.

first form at some distance from the preceding one. Once a critical crack density is reached (which is dependent on the film material, substrate, and film thickness), the stress relaxation zones of neighboring cracks overlap, preventing the stress within the film fragment between them from reaching the critical value required to form a new crack.

Our analysis indicates that the maximum critical strain that an a-olivine thin film can withstand is approximately 0.8 %. Using a Young's modulus of 90 GPa (Baral et al., 2021) and assuming linear elastic behavior prior to fracture, one can estimate the strength of 720 MPa for a-olivine films. However, the macroscopic mechanical behavior of the film is significantly influenced by the presence of defects, some of which are marked in Fig. 2a. These defects are inherent for films synthesized by physical vapor deposition and can stem from different origins, such as surface contamination, substrate imperfections, electric arcs during deposition, or seed particles (Panjan et al., 2020). Local stress in the vicinity of the defect can be several times higher than the average global stress within the film, which results in the initiation

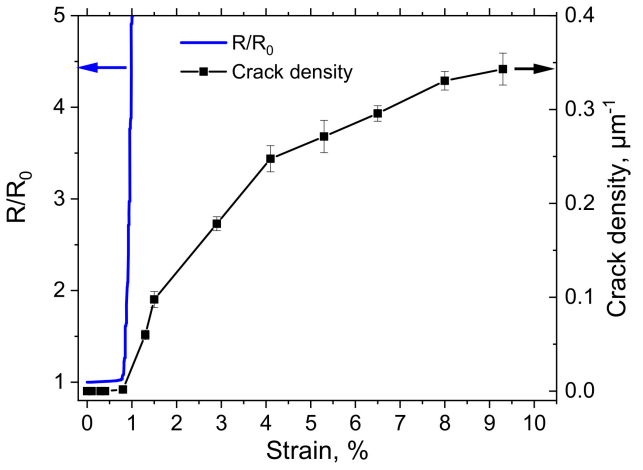

Figure 4. The evolution of in situ resistance (left y axis, blue curve) and crack density (right y axis, black curve and symbols) of gold-covered a-olivine films on a polymer substrate with increasing strain. The measured resistance R is normalized to the initial resistance at zero strain R_0.

of cracks, as illustrated in Fig. 2a. Once initiated, the stress concentration on the crack tips drives them to propagate over long distances due to the absence of plasticity mechanisms at room temperature and the absence of microstructural obstacles (e.g., grain boundaries) in a-olivine. Therefore, the measured critical strain should be considered an extrinsic property that is strongly influenced by the density and size of the stress-concentrating defects.

In order to estimate the intrinsic strength of a-olivine, we employed a methodology based on DIC using the images obtained from in situ CLSM experiments. The analysis was specifically focused on the local strains within the intact fragments of the film between the cracks. Figure 5a illustrates the averaged values of the major strain ε_{yy} and minor strain ε_{xx} in the central region of nine film fragments from three different samples, plotted as thin grey lines, depending on the applied global strain. The mean of the nine individual curves is showed by the red curve for ε_{yy} and the blue curve for ε_{xx}. Figure 5b illustrates the distribution of local strains at varying values of applied global strain for a single film fragment. The color code represents the magnitude of the local major strain component ε_{yy}, as indicated in the accompanying legend. The first strain map marked by a capital "A" was obtained prior to the formation of cracks within the region of interest. In the subsequent maps (marked with "B", "C", and "D"), the DIC software was unable to compute the local strain in the vicinity of the cracks due to their emergence as new objects that were not present in the original image prior to straining. In accordance with the shear lag model, the maximum strain within a film fragment is anticipated to be in the middle between two cracks (Ahmed et al., 2011; Hsueh and Yanaka, 2003). Therefore, the local strain values depicted in Fig. 5a are calculated by averaging the strain along a line situated in the center of each fragment between two cracks, as illustrated in Fig. 5b by dotted lines. It should be noted that the evolution of local strain in Fig. 5a is captured until the global strain of approximately 6 %. At higher applied strains, further fracture events make the size of the intact film fragments comparable to the subset size of the DIC analysis, and the local strains cannot be measured. Although with additional and specifically designed speckle patterns it might be possible to also resolve local strains within smaller film fragments, the physical limitations of optical microscopy would not allow for a significant increase in the spatial resolution of the strain map.

As illustrated in Fig. 5a, the ε_{yy} component reaches values that are markedly higher than the macroscopic COS of 0.8 %, substantiating the assertion that a-olivine is capable of sustaining tensile strains in excess of 2 %. The transverse compressive strain (ε_{xx}) also reaches substantial values of above 1 %. The evolution of the tensile strain component ε_{yy} of individual film fragments is characterized by a large spread and zigzag behavior with increasing applied strain. This can be explained by the fact that the formation of each crack results in strain relaxation in the tensile direction. Therefore, each film fragment has a different history of crack propagation in its vicinity, resulting in different evolutionary trends of local tensile strain as well as in heterogeneous crack spacing. In contrast, the transverse compressive component ε_{xx} exhibits excellent repeatability across different specimens and film fragments. This is due to the fact that the transverse compression is controlled by the global strain state resulting from the discrepancies in Poisson contraction between the film and the substrate. At the same time, the formation of cracks perpendicularly to the straining direction has a negligible impact on the local transverse compression state. The Poisson ratio of a-olivine is 0.37 (Baral et al., 2021), whereas that of polyimide depends on the applied strain, exhibiting a value of approximately 0.34 below 1 % strain and reaching a value of 0.48 at 3.8 % strain (Bauer and Farris, 1989). This effect of the strain-dependent Poisson ratio of polyimide can be observed in the behavior of the ε_{xx} component. At low strains, the substrate exhibits a lower Poisson ratio than the film, resulting in minimal growth of compressive strain within the film. However, at strains exceeding 1 %, the significantly higher Poisson ratio of the substrate leads to a notable increase in compressive strain imposed on the film.

As DIC captures the total surface strains, it is not possible to differentiate directly between elastic and plastic deformation. Accordingly, in order to ascertain the material strength on the basis of the measured surface strains, it is imperative to demonstrate that no significant local plasticity has occurred within the fragments, at least in the context of the prevailing testing conditions. In light of the absence of substantial evidence of plasticity as illustrated in Fig. 3 and the corresponding discussion of it, it appears reasonable to conclude that the strains measured with DIC are of an elastic nature. It can thus be stated that the intrinsic tensile strength of a-

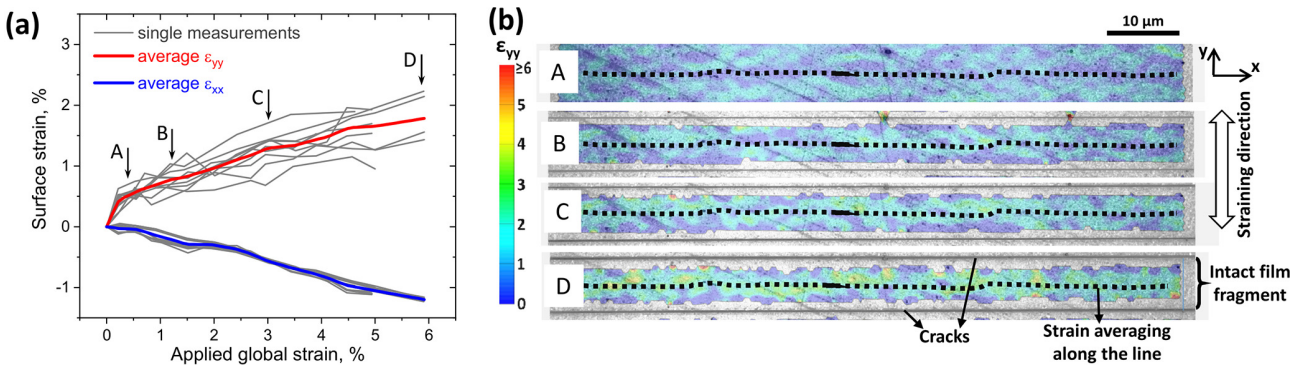

Figure 5. Measurements of local strain in polymer-supported a-olivine film using DIC. **(a)** Evolution of the major tensile (ε_{yy}) and transverse compressive (ε_{xx}) strain components in the middle of intact film fragments with increasing global applied strain. The grey lines represent nine single measurements from three different samples. The thick red and blue lines are averaged evolution for ε_{yy} and ε_{xx} strain components, respectively. The vertical arrows with capital letters mark the global strains corresponding to the strain maps shown in **(b)**. **(b)** Exemplary distribution of the major strain (ε_{yy}) within a film fragment at different applied strains marked by corresponding capital letters in **(a)**.

olivine is at least 1.8 GPa (based on 2 % local strain and a modulus of 90 GPa; Baral et al., 2021). Concurrently, the a-olivine films underwent transverse compressive strain of up to 1.2 %, thus exhibiting a complex bi-axial strain state.

The methodology proposed here can be considered an uncontrolled microtensile test applied to stochastically formed film fragments. A significant limitation of this microtensile test is its inability to control the applied load and to measure a stress–strain curve. However, the method offers several advantages beyond its straightforward and time-effective preparation and testing procedure. First, the effect of stress-concentrating defects is mitigated in a natural manner. Substantial stress-concentrating defects have already initiated a crack and are thus automatically excluded from the consideration. The principal benefit of utilizing a polymer-supported film is that substantial statistical data can be rapidly accumulated by considering a multitude of intact film fragments within a single macroscopic specimen. Ultimately, a full in-plane strain tensor is measured (i.e., ε_{yy}, ε_{xx}, and ε_{xy} components), opening up a possibility of applying material-specific failure criteria (von Mises, Mohr–Coulomb, etc.) or calculating locally stored elastic strain energy.

In recent microtensile experiments, the tensile strength of freestanding a-olivine films was found to be up to 1.5 GPa, with a directly observed maximal strain without fracture of 1.8 % (Coulombier et al., 2024). It is noteworthy that these experiments employed extremely low strain rates, reaching as low as $10^{-12}\,s^{-1}$, i.e., many orders of magnitude below the strain rates of the current work. Nevertheless, our estimation of critical tensile strain of 2 % aligns well with the findings of micromechanical experiments (Coulombier et al., 2024).

In this study we have characterized the tensile strength of a-olivine at room temperature. The critical parameter that determines whether an amorphous material behaves brittly and fractures or behaves like a fluid and flows is the glass transition temperature, T_g (Angell et al., 2000). The glass transition temperature of amorphous olivine is $1263 \pm 10\,°C$ (Richet et al., 1993), and a-olivine is expected to exhibit this brittle behavior in the coldest part of the lithospheric mantle. In polycrystalline olivine experiencing stress-induced amorphization, a-olivine appears in the form of ultrathin intercrystalline thin film (Samae et al., 2021). At such a small scale, even nominally brittle materials can demonstrate significant plasticity, as has been demonstrated for Al_2O_3 (Frankberg et al., 2019), MgO (Issa et al., 2015), or silicon (Issa et al., 2021) and for a-olivine itself (Orekhov et al., 2024). Given the strong confinement and absence of a free surface, it is reasonable to conclude that the propagation of cracks in such small-scale a-olivine layers is also prohibited. It is therefore anticipated that the mechanical behavior of a-olivine in amorphized grain boundaries will be defined by its intrinsic strength and its relation to the characteristic properties of surrounding crystalline olivine. Compared to natural conditions, our measurements are also made at ambient pressure. Pressure has been shown to have a moderate effect on the rheology of a-olivine (Delbecq et al., 2023), and it is expected that the intrinsic strength is little or not affected by pressures in the lithosphere. For brittle solids, the tensile strength is usually lower than the shear and compressive strengths. The properties determined in this study can be considered a lower limit for the behavior of a-olivine. Pressure inhibits brittleness, but at high stress, near the brittle–ductile transition, tensile components can be locally found in polycrystalline aggregates even under confining pressure. This can be the case not only in the vicinity of pores or heterogeneities (Bernabé and Peč, 2024), but also in the presence of incompatibilities in the vicinity of triple joints in polycrystals that deform by grain boundary sliding (Beeré, 1978), a mechanism that has been shown to operate in olivine, even under pressure (Bollinger et al., 2019). Since deformation and fracture always occur along the weakest path following the principle of energy minimization, the measured intrinsic strength of a-

olivine should assist in better understanding of whether the grain boundaries, grain boundaries containing a-olivine, or grain interior will be the "weak link" initiating or promoting rock failure.

4 Summary and conclusions

The mechanical behavior of polymer-supported a-olivine thin films was characterized using a tensile test with in situ resistance measurements and a tensile test with in situ optical microscopy combined with DIC analysis. It is demonstrated that the cracks are initiated at an applied strain of approximately 0.8 % due to the presence of numerous defects that act as stress concentration points and sites of crack initiation. Macroscopically, a-olivine exhibits a typical brittle fracture morphology manifested by long, straight, and parallel cracks. A novel methodology for capturing the evolution of maximal local strains within the intact film fragments as a function of increasing global strain was introduced, enabling the estimation of the intrinsic strength of a-olivine. It was demonstrated that a-olivine can withstand tensile strains of up to 2 %, corresponding to a strength of approximately 1.8 GPa, assuming that the measured strains are of elastic nature.

Data availability. The data that support the findings of this study are available from the corresponding author upon reasonable request.

Video supplement. The video shows the sequence of optical images taken during the tensile test of a polymer-supported amorphous olivine film. The thickness of the film is about 100 nm; the thickness of the polyimide substrate is 50 µm. The straining direction is vertical. With increasing applied strain, cracks in the form of long straight lines appear. The crack density increases with increasing strain and is saturated at higher strains, as is typical for intrinsically brittle polymer-supported films. The online video supplement is available at https://doi.org/10.5446/69638 (Glushko, 2024).

Supplement. The supplement related to this article is available online at https://doi.org/10.5194/ejm-37-91-2025-supplement.

Author contributions. JJ: investigation, validation, visualization, formal analysis; RD: investigation, resources, writing (review and editing); COWT: investigation, writing (review and editing); CM: resources, writing (review and editing); PC: conceptualization, validation, writing (original draft, review and editing); OG: conceptualization, methodology, investigation, visualization, validation, writing (original draft, review and editing).

Competing interests. The contact author has declared that none of the authors has any competing interests.

Disclaimer. Publisher's note: Copernicus Publications remains neutral with regard to jurisdictional claims made in the text, published maps, institutional affiliations, or any other geographical representation in this paper. While Copernicus Publications makes every effort to include appropriate place names, the final responsibility lies with the authors.

Acknowledgements. Oleksandr Glushko would like to acknowledge financial support provided by the Austrian Science Fund (FWF) and Land Steiermark through project no. P31544-NBL. Patrick Cordier has received funding from the European Research Council (ERC) under the European Union's Horizon 2020 research and innovation program under grant agreement no. 787198 – TimeMan.

Financial support. This research has been supported by the Austrian Science Fund (grant no. P31544-NBL). Patrick Cordier has received funding from the European Research Council (ERC) (grant no. 787198).

Review statement. This paper was edited by Tiziana Boffa Ballaran and reviewed by Matej Pec and one anonymous referee.

References

Ahmed, F., Bayerlein, K., Rosiwal, S. M., Göken, M., and Durst, K.: Stress evolution and cracking of crystalline diamond thin films on ductile titanium substrate: Analysis by micro-Raman spectroscopy and analytical modelling, Acta Mater., 59, 5422–5433, https://doi.org/10.1016/j.actamat.2011.05.015, 2011.

Andrault, D., Bouhifd, M. A., Itié, J. P., and Richet, P.: Compression and amorphization of $(Mg,Fe)_2SiO_4$ olivines: An X-ray diffraction study up to 70 GPa, Phys. Chem. Miner., 22, 99–107, https://doi.org/10.1007/BF00202469, 1995.

Angell, C. A., Ngai, K. L., McKenna, G. B., McMillan, P. F., and Martin, S. W.: Relaxation in glassforming liquids and amorphous solids, J. Apl. Phys., 88, 3113–3157, 2000.

Austrheim, H. and Andersen, T. B.: Pseudotachylytes from Corsica: fossil earthquakes from a subduction complex, Terra Nov., 16, 193–197, https://doi.org/10.1111/j.1365-3121.2004.00551.x, 2004.

Baral, P., Orekhov, A., Dohmen, R., Coulombier, M., Raskin, J. P., Cordier, P., Idrissi, H., and Pardoen, T.: Rheology of amorphous olivine thin films characterized by nanoindentation, Acta Mater., 219, 117257, https://doi.org/10.1016/j.actamat.2021.117257, 2021.

Bauer, C. L. and Farris, R. J.: Determination of poisson's ratio for polyimide films, Polym. Eng. Sci., 29, 1107–1110, https://doi.org/10.1002/pen.760291606, 1989.

Beeré, W.: Stresses and deformations at grain boundaries, Philos. T. R. Soc. Lond. A, 288, 177–196, 1978.

Bernabé, Y. and Peč, M.: Brittle damage processes around equi-dimensional pores or cavities in rocks: Implications for the brittle-ductile transition, J. Geophys. Res.-Sol. Ea., 129, e2024JB028814, https://doi.org/10.1029/2024JB028814, 2024.

Bollinger, C., Marquardt, K., and Ferreira, F.: Intragranular plasticity vs. grain boundary sliding (GBS) in forsterite: Microstructural evidence at high pressures (3.5–5.0 GPa), Am. Mineral., 104, 220–231, 2019.

Coulombier, M., Baral, P., Orekhov, A., Dohmen, R., Raskin, J. P., Pardoen, T., Cordier, P., and Idrissi, H.: On-chip very low strain rate rheology of amorphous olivine films, Acta Mater., 266, 119693, https://doi.org/10.1016/j.actamat.2024.119693, 2024.

Darot, M., Gueguen, Y., Benchemam, Z., and Gaboriaud, R.: Ductile-brittle transition investigated by micro-indentation: results for quartz and olivine, Phys. Earth Planet. In., 40, 180–186, https://doi.org/10.1016/0031-9201(85)90128-1, 1985.

Delbecq, V., Carrez, P., and Cordier, P.: Rheological properties of Mg_2SiO_4 glass: A molecular dynamics study, J. Non-Cryst. Sol., 619, 122572, https://doi.org/10.1016/j.jnoncrysol.2023.122572, 2023.

Dohmen, R., Chakraborty, S., and Becker, H. W.: Si and O diffusion in olivine and implications for characterizing plastic flow in the mantle, Geophys. Res. Lett., 29, 26-1-26–4, https://doi.org/10.1029/2002GL015480, 2002.

Druiventak, A., Trepmann, C. A., Renner, J., and Hanke, K.: Low-temperature plasticity of olivine during high stress deformation of peridotite at lithospheric conditions – An experimental study, Earth Planet. Sc. Lett., 311, 199–211, https://doi.org/10.1016/j.epsl.2011.09.022, 2011.

Frankberg, E. J., Kalikka, J., Ferré, F. G., Joly-Pottuz, L., Salminen, T., Hintikka, J., Hokka, M., Koneti, S., Douillard, T., Le Saint, B., Kreiml, P., Cordill, M. J., Epicier, T., Stauffer, D., Vanazzi, M., Roiban, L., Akola, J., Fonzo, F. D., Levänen, E., and Masenelli-Varlot, K.: Highly ductile amorphous oxide at room temperature and high strain rate, Science, 366, 864–869, https://doi.org/10.1126/science.aav1254, 2019.

Gasc, J., Demouchy, S., Barou, F., Koizumi, S., and Cordier, P.: Creep mechanisms in the lithospheric mantle inferred from deformation of iron-free forsterite aggregates at 900–1200 °C, Tectonophysics, 761, 16–30, https://doi.org/10.1016/j.tecto.2019.04.009, 2019.

Glushko, O.: In-situ tensile test of amorphous olivine film, TIB-AV Portal [video], https://doi.org/10.5446/69638, 2024.

Glushko, O. and Cordill, M. J.: Electrical Resistance of Metal Films on Polymer Substrates Under Tension, Exp. Techniques, 40, 303–310, https://doi.org/10.1007/s40799-016-0040-x, 2016.

Goldsby, D. L. and Tullis, T. E.: Low frictional strength of quartz rocks at subseismic slip rates, Geophys. Res. Lett., 29, 24–25, https://doi.org/10.1029/2002GL015240, 2002.

Hayward, K. S., Cox, S. F., Fitz Gerald, J. D., Slagmolen, B. J. J., Shaddock, D. A., Forsyth, P. W. F., Salmon, M. L., and Hawkins, R. P.: Mechanical amorphization, flash heating, and frictional melting: Dramatic changes to fault surfaces during the first millisecond of earthquake slip, Geology, 44, 1043–1046, https://doi.org/10.1130/G38242.1, 2016.

Hsueh, C. H. and Yanaka, M.: Multiple film cracking in film/substrate systems with residual stresses and unidirectional loading, J. Mater. Sci., 38, 1809–1817, https://doi.org/10.1023/A:1023200415364, 2003.

Issa, I., Amodeo, J., Réthoré, J., Joly-Pottuz, L., Esnouf, C., Morthomas, J., Perez, M., Chevalier, J., and Masenelli-Varlot, K.: In situ investigation of MgO nanocube deformation at room temperature, Acta Mater., 86, 295–304, https://doi.org/10.1016/j.actamat.2014.12.001, 2015.

Issa, I., Gammer, C., Kolitsch, S., Hohenwarter, A., Imrich, P. J., Pippan, R., and Kiener, D.: In-situ TEM investigation of toughening in Silicon at small scales, Mater. Today, 48, 29–37, https://doi.org/10.1016/j.mattod.2021.03.009, 2021.

Janssen, C., Wirth, R., Rybacki, E., Naumann, R., Kemnitz, H., Wenk, H.-R., and Dresen, G.: Amorphous material in SAFOD core samples (San Andreas Fault): Evidence for crush-origin pseudotachylytes?, Geophys. Res. Lett., 37, L01303, https://doi.org/10.1029/2009GL040993, 2010.

Jörg, T., Cordill, M. J., Franz, R., Kirchlechner, C., Többens, D. M., Winkler, J., and Mitterer, C.: Thickness dependence of the electro-mechanical response of sputter-deposited Mo thin films on polyimide: Insights from in situ synchrotron diffraction tensile tests, Mater. Sci. Eng. A, 697, 17–23, https://doi.org/10.1016/j.msea.2017.04.101, 2017.

Kaneki, S., Oohashi, K., Hirono, T., and Noda, H.: Mechanical Amorphization of Synthetic Fault Gouges During Rotary-Shear Friction Experiments at Subseismic to Seismic Slip Velocities, J. Geophys. Res.-Sol. Ea., 125, e2020JB019956, https://doi.org/10.1029/2020JB019956, 2020.

Kiener, D. and Misra, A.: Nanomechanical characterization, MRS Bull., 49, 1–10, https://doi.org/10.1557/s43577-023-00643-z, 2023.

Kranjc, K., Thind, A. S., Borisevich, A. Y., Mishra, R., Flores, K. M., and Skemer, P.: Amorphization and Plasticity of Olivine During Low-Temperature Micropillar Deformation Experiments, J. Geophys. Res.-Sol. Ea., 125, 1–12, https://doi.org/10.1029/2019JB019242, 2020.

Latella, B. A., Triani, G., Zhang, Z., Short, K. T., Bartlett, J. R., and Ignat, M.: Enhanced adhesion of atomic layer deposited titania on polycarbonate substrates, Thin Solid Films, 515, 3138–3145, https://doi.org/10.1016/j.tsf.2006.08.022, 2007.

Niemeijer, A., Di Toro, G., Nielsen, S., and Di Felice, F.: Frictional melting of gabbro under extreme experimental conditions of normal stress, acceleration, and sliding velocity, J. Geophys. Res.-Sol. Ea., 116, https://doi.org/10.1029/2010JB008181, 2011.

Obata, M. and Karato, S.: Ultramafic pseudotachylite from the Balmuccia peridotite, Ivrea-Verbano zone, northern Italy, Tectonophysics, 242, 313–328, https://doi.org/10.1016/0040-1951(94)00228-2, 1995.

Orekhov, A., Kermouche, G., Gomez-Perez, A., Baral, P., Dohmen, R., Coulombier, M., Verbeeck, J., Pardoen, T., Schryvers, D., Lin, J., Cordier, P., and Idrissi, H.: Room temperature electron beam sensitive viscoplastic response of ultraductile amorphous olivine films, Acta Mater., 282, 120479, https://doi.org/10.1016/j.actamat.2024.120479, 2024.

Pan, Z. and Rupert, T. J.: Amorphous intergranular films as toughening structural features, Acta Mater., 89, 205–214, https://doi.org/10.1016/j.actamat.2015.02.012, 2015.

Panjan, P., Drnovšek, A., Gselman, P., Čekada, M., and Panjan, M.: Review of growth defects in thin films prepared by PVD techniques, Coatings, 10, 447, https://doi.org/10.3390/COATINGS10050447, 2020.

Park, J. W., Kim, G., Lee, S. H., Kim, E. H., and Lee, G. H.: The effect of film microstructures on cracking of transparent conductive oxide (TCO) coatings on poly-

mer substrates, Surf. Coatings Technol., 205, 915–921, https://doi.org/10.1016/j.surfcoat.2010.08.055, 2010.

Pec, M., Stünitz, H., Heilbronner, R., Drury, M., and de Capitani, C.: Origin of pseudotachylites in slow creep experiments, Earth Planet. Sci. Lett., 355/356, 299–310, https://doi.org/10.1016/j.epsl.2012.09.004, 2012.

Peng, C., Jia, Z., Bianculli, D., Li, T., and Lou, J.: In situ electro-mechanical experiments and mechanics modeling of tensile cracking in indium tin oxide thin films on polyimide substrates, J. Appl. Phys., 109, 1–8, https://doi.org/10.1063/1.3592341, 2011.

Richet, P., Leclerc, F., and Benoist, L.: Melting of forsterite and spinel, with implications for the glass transition of Mg_2SiO_4 liquid, Geophys. Res. Lett., 20, 1675–1678, 1993.

Samae, V., Cordier, P., Demouchy, S., Bollinger, C., Gasc, J., Koizumi, S., Mussi, A., Schryvers, D., and Idrissi, H.: Stress-induced amorphization triggers deformation in the lithospheric mantle, Nature, 591, 82–86, https://doi.org/10.1038/s41586-021-03238-3, 2021.

Scambelluri, M., Pennacchioni, G., Gilio, M., Bestmann, M., Plümper, O., and Nestola, F.: Fossil intermediate-depth earthquakes in subducting slabs linked to differential stress release, Nat. Geosci., 10, 960–966, https://doi.org/10.1038/s41561-017-0010-7, 2017.

Wenk, H. R.: Are pseudotachylites products of fracture or fusion?, Geology, 6, 507–511, https://doi.org/10.1130/0091-7613(1978)6<507:APPOFO>2.0.CO;2, 1978.

Yund, R. A., Blanpied, M. L., Tullis, T. E., and Weeks, J. D.: Amorphous material in high strain experimental fault gouges, J. Geophys. Res.-Sol. Ea., 95, 15589–15602, https://doi.org/10.1029/JB095iB10p15589, 1990.